Accepted Manuscript

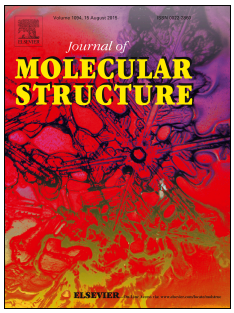

Tautomerism in *N*-(2-hydroxy-1-naphthylidene)amino acids and the search for an answer to the difficult question about where the proton belongs

Gisela Warncke, Sabine Fels, Erica Brendler, Uwe Böhme

PII: S0022-2860(16)30235-6

DOI: 10.1016/j.molstruc.2016.03.040

Reference: MOLSTR 22351

To appear in: *Journal of Molecular Structure*

Received Date: 14 December 2015

Revised Date: 14 March 2016

Accepted Date: 14 March 2016

Please cite this article as: G. Warncke, S. Fels, E. Brendler, U. Böhme, Tautomerism in *N*-(2-hydroxy-1-naphthylidene)amino acids and the search for an answer to the difficult question about where the proton belongs, *Journal of Molecular Structure* (2016), doi: 10.1016/j.molstruc.2016.03.040.

Graphical Abstract

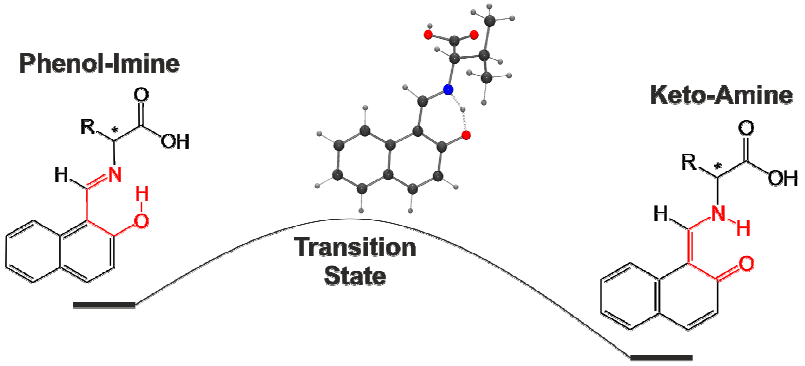

Tautomerism in *N*-(2-hydroxy-1-naphthylidene)amino acids and the search for an answer to the difficult question about where the proton belongs

Gisela Warncke[a], *Sabine Fels*[a], *Erica Brendler*[b], *Uwe Böhme*[a]*

[a] TU Bergakademie Freiberg, Institut für Anorganische Chemie, Leipziger Straße 29, 09596 Freiberg. Tel: +49 3731 39 2050; Fax: +49 3731 394058.

[b] TU Bergakademie Freiberg, Institut für Analytische Chemie, Leipziger Straße 29, 09596 Freiberg. Tel: +49 3731 39 2266; Fax: +49 3731 393666.

* E-Mail: Uwe.Boehme@chemie.tu-freiberg.de.

Abstract

N-(2-hydroxy-1-naphthylidene)-L-valine **1**, *N*-(2-hydroxy-1-naphthylidene)-L-phenylalanine **2**, and *N*-(2-hydroxy-1-naphthylidene)-L-threonine **3** were prepared and characterized with spectroscopic methods, elemental analyses, and values of optical rotation. Compound **1** undergoes a solid state order-disorder phase transition at 231 K. The X-ray structures of the high and low temperature phase of **1** have been determined. Single crystal X-ray structures of **2** and **3** have been determined as well. The tautomerism of *N*-(2-hydroxy-1-naphthylidene)amino acid derivatives is discussed controversial in the literature. A bond lengths statistical analysis shows that all three compounds exist uniformly in the keto-amine form in the solid state. Quantum chemical calculations, NMR, and UV-Vis spectroscopy were used to obtain further insight into the existence of phenol-imine and keto-amine structures in this class of compounds.

Keywords: Schiff base, chiral ligand, tautomerism, X-ray structure, NMR spectroscopy

1. Introduction

Schiff base ligands have proven useful in silicon and tin complex formation, with the products showing antimicrobial [1], bacteriostatic [2], bacteriocidal [3], biocidal [4] and fungicidal [5, 6] properties as well as antitumor activity [6]. After research on Salen-type [7, 8, 9, 10,] and tridentate O,N,O'-ligands in silicon and tin complexes [11, 12, 13, 14, 15,] we are working on hypercoordinated silicon and tin complexes with chiral ligands [16, 17, 18]. Our recent work is focused on 2-hydroxynaphthaldehyde derivatives shown in Figure 1 [19]. Such ligands are already known for their complexation abilities for lanthanum and cerium [20], zirconium [21], manganese [22, 23, 24, 25, 26], iron [27, 28, 29], cobalt [30], nickel [31, 30], copper [32, 30], zinc [33], cadmium [33], silicon [1], and tin [19, 34].

In contrast to the interest in the coordination chemistry of *N*-(2-hydroxy-1-naphtylidene)amino acids only a few papers deal with characterization and properties of the free Schiff bases [29, 35]. This may arise from the fact that in many studies the Schiff bases are formed *in situ* during the complexation reactions. Herein we report the syntheses and characterization of three *N*-(2-hydroxy-1-naphthylidene)amino acids (Figure 1). The question whether these compounds exist in phenol-imine form (**PI)** or keto-amine form (**KA)** in the solid state is investigated on the basis of the X-ray structural data in combination with bond lengths statistics drawn from the Cambridge Structural Database. NMR and UV-Vis spectroscopy were used to obtain further insight into the occurrence of the tautomeric forms in solution and quantum chemical calculations to discover the relation between these two tautomers.

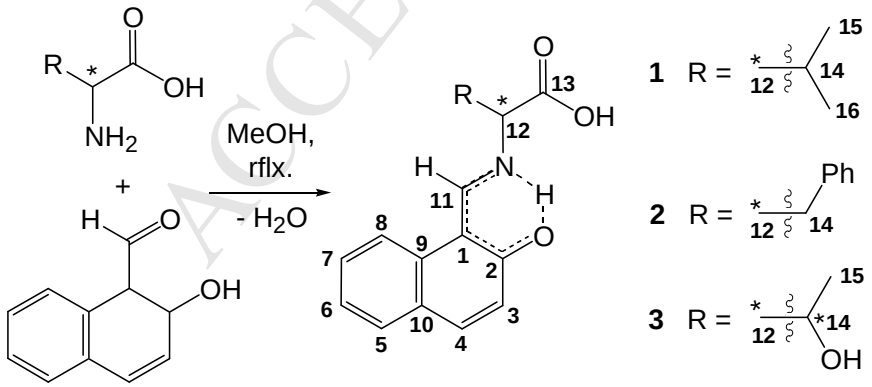

Figure1: Preparation of 2-hydroxy-1-naphthylidene-amino acids **1**, **2** and **3** from L-valine (R = *i*-propyl), L-phenylalanine (R = CH_2-Ph), and L-threonine (R = *CHOH-CH_3), respectively.

2. Experimental

2.1 Materials and Methods

The necessary chemicals were used as commercially available. Solvents were dried according to standard procedures. Melting points were determined with a Polytherm A from Wagner & Munz using samples in sealed capillaries.

Solution state NMR spectra were recorded on a Bruker DPX 400 and Avance III 500 spectrometer at 293 K [^{1}H (400.13 MHz), ^{13}C (100.61 MHz) and ^{1}H (500.13 MHz), ^{13}C (125.76 MHz), respectively] with tetramethylsilane as internal standard. The concentration of the samples varied from 0.4 to 40 mg/ ml depending on solubility and scope of measurement, for routine characterization 10 mg /ml were used. 8 to 128 (^{1}H) and 128 to 16 k (^{13}C) scans were accumulated, 2D spectra were recorded with 128 or 256 t1-increments. The assignment of the signals was performed using H,H-COSY, H,H-NOESY, H,C-HSQC and HMBC experiments and is consistent to the assignment made by Rozwadowski et al. [36].

^{13}C CP MAS NMR measurements were carried out at 100.6 MHz on a Bruker AVIII HD 400 WB spectrometer with a DVT probe using 4 mm ZrO_2 rotors at 10 kHz spinning speed. A contact time of 2 ms with an 70% ramp on the ^{1}H channel was applied for CP, experiment recycle delay of 5 s, 1k scans and an acquisition time of 50 ms with tppm15 decoupling were used. The chemical shift was referenced externally using the CH-group signal of adamantane (38.5 ppm with respect to TMS= 0 ppm).

Elemental analyses were performed with Foss Heraeus CHN-O-Rapid, UV-Vis spectra with Jasco V-650 spectrophotometer, and Polarimetry with Perkin Elmer Polarimeter 241. Concentration of UV-Vis samples were 0.2 mmol/l. The stability of optical rotation values has been tested up to 120 hours after preparing the solution. No substantial deviations were observed within experimental error of ±0.5°.

*2.2 Synthesis of N-(2-hydroxy-1-naphthylidene)-L-valine (**1**)*

2-Hydroxy-1-naphthaldehyde (30 mmol, 2.58 g) was added to a suspension of L-valine (20 mmol, 1.17 g) in methanol/ethanol (20 ml/250 ml). The reaction mixture was stirred under reflux for 6 h, while it slowly turned yellow. After cooling to room temperature, the solution was stirred at room temperature for another 24 hours. The reaction mixture was filtered and the yellow solution concentrated in vacuo. Diethyl ether (100 ml) was added to the yellow solid and stirred at room temperature in order to remove 2-hydroxy-1-naphthaldehyde. The yellow suspension was filtered. The remaining yellow solid was washed with diethyl ether and dried in vacuo. Yield: 4.40 g (81%). m.p. = 185-189 °C (literature [35] 187 °C). ^{1}H NMR

(DMSO, ppm): δ = 14.49 (s, 1H, C2-OH), 13.37 (s, 1H, C13-OH), 9.15 (s, 1H, H11), 8.07 (d, 1H, H8, $^{3}J_{H-H}$ = 8.4 Hz), 7.77 (d, 1H, H4, $^{3}J_{H-H}$ = 9.3 Hz), 7.66 (dd, 1H, H5, $^{3}J_{H-H}$ = 7.9 Hz, $^{4}J_{H-H}$ = 1.3 Hz), 7.43 (m, 1H, H7, $^{3}J_{H-H}$ = 8.4 Hz, 7 Hz, $^{4}J_{H-H}$ = 1.3 Hz), 7.22 (m, 1H, H6, $^{3}J_{H-H}$ = 7 Hz, 7.9 Hz, $^{4}J_{H-H}$ = 1 Hz), 6.78 (d, 1H, H3, $^{3}J_{H-H}$ = 9.3 Hz), 4.34 (d, 1H, H12, $^{3}J_{H-H}$ = 4.3 Hz), 2.34 (m, 1H, H14, $^{3}J_{H-H}$ = 4.3 Hz, $^{3}J_{H-H}$ = 6.9 Hz); 0.96 (d, 6H, H15/H16, $^{3}J_{H-H}$ = 6.9 Hz). ^{13}C NMR (δ, ppm): δ = 176.1 (C2), 171.8 (C13), 159.7 (C11), 137.2 (C4), 134.1 (C9), 129 (C5), 128 (C7), 125.5 (C10), 124.8 (C3), 122.5 (C6), 118.6 (C8), 106.3 (C1), 69.3 (C12), 31.1 (C14), 17.1/18.9 (C15/C16). ^{13}C CP/MAS NMR (δ, ppm): δ = 178.6 (C2), 175.0 (C13), 161.0 (C11), 137.7 (C4), 134.4 (C9), 128.2 (C5), 127.0 (C7), 125.7 (C10), 123.4 (C3), 122.3 (C6), 118.3 (C8), 106.3 (C1), 68.1 (C12), 32.7 (C14), 22.2 (C15/C16).
$[\alpha]_D^{20}$ = -109° (0.1 g / 100 ml DMSO). UV-Vis in DMSO, λ [nm] (ε in l/(mol*cm)): 307 (11840), 403 (10150), 423 (10340). Anal. calcd. for $C_{16}H_{17}NO_3$: C 70.83, H 6.32, N 5.16; found: C 70.78, H 6.26, N 5.15.

*2.3 Synthesis of N-(2-hydroxy-1-naphthylidene)-L-phenylalanine (**2**)*

2-Hydroxy-1-naphthaldehyde (22.5 mmol, 3.87 g) was added to a suspension of L-phenylalanine (15 mml, 2.48 g) in methanol/ethanol (20 ml/150 ml). The yellow suspension was stirred at room temperature for 18 h, followed by 6 hours under reflux. After one hour a yellow precipitate formed from the hot yellow solution. After cooling to room temperature, the solution was stirred at room temperature for two more days. The solid was filtered, washed twice with 10 ml methanol and dried in vacuo. Yield: 3.58 g (75%). m.p. = 184-186 °C (literature [35] 170 °C). . ^{1}H NMR (DMSO, ppm): δ = 14.29 (s, 1H, C2-OH), 13.44 (s, 1H, C13-OH), 8.95 (s, 1H, H11), 7.90 (d, 1H, H8, $^{3}J_{H-H}$ = 8.4 Hz), 7.76 (d, 1H, H4, $^{3}J_{H-H}$ = 9.3 Hz), 7.66 (dd, 1H, H5, $^{3}J_{H-H}$ = 7.9 Hz, $^{4}J_{H-H}$ = 1.4 Hz), 7.43 (m, 1H, H7, $^{3}J_{H-H}$ = 7 Hz; 8.4 Hz, $^{4}J_{H-H}$ = 1.4 Hz), 7.30-7.18 (m, 6H, Ph-H_{ar} + H6), 6.78 (d, 1H, H3, $^{3}J_{H-H}$ = 9.3 Hz), 4.77 (dd, 1H, H12, $^{3}J_{H-H}$ = 5.0 Hz; 8.3 Hz), 3.37 (dd, 1H, H14b, $^{3}J_{H-H}$ = 5.0 Hz, $^{2}J_{H-H}$ = 13.9 Hz), 3.20 (dd, 1H, H14a, $^{3}J_{H-H}$ = 8.3 Hz, $^{2}J_{H-H}$ = 13.9 Hz). ^{13}C NMR (DMSO, ppm): δ = 174.9 (C2), 171.7 (C13), 159.5 (C11), 137 (C4), 136.4 (*ipso*-Ph), 133.8 (C9), 129.5 (*o*-Ph), 128.9 (C5), 128.4 (*m*-Ph), 127.9 (C7), 126.8 (*p*-Ph), 125.6 (C10), 124.3 (C3), 122.6 (C6), 118.6 (C8), 106.2 (C1), 65.2 (C12). $[\alpha]_D^{20}$ = 0° (1 g / 100 ml DMSO). UV-Vis in DMSO, λ [nm] (ε in l/(mol*cm)): 307 (14840), 404 (11030), 425 (11180). Anal. calcd. for CHNO: C 75.22, H 5.37, N 4.39; found: C 72.67, H 5.01, N 4.25.

*2.4 Synthesis of N-(2-hydroxy-1-naphthylidene)-L-threonine (**3**)*

2-Hydroxy-1-naphthaldehyde (20 mmol, 3.40g) was dissolved in methanol (200 ml). L-threonine (20 mmol, 2.40g) was added and the reaction mixture was stirred under reflux for 3 h. The yellow solution was filtered and allowed to cool to room temperature. While standing overnight, fine yellow needles crystallized and were collected for x-ray diffraction analysis. The yellow solution was concentrated in a vacuum to on third of its volume whereby a yellow solid precipitated. The solid was filtered off and dried in a desiccator in vacuum over $CaCl_2$. Yield: 3.16g (58%). m.p. = 188-190 °C. ^{1}H NMR (DMSO, ppm): δ = 13.82 (s, 1H, C2-OH), 13.11 (s, 1H; C13-OH), 9.02 (s, 1H, H11), 7.98 (d, 1H, H8, $^3J_{H-H}$ = 8.4 Hz), 7.72 (d, 1H, H4, $^3J_{H-H}$ = 9.4 Hz), 7.61 (dd, 1H, H5, $^3J_{H-H}$ = 7.9 Hz, $^4J_{H-H}$ = 1.4 Hz), 7.41 (m, 1H, H7, $^3J_{H-H}$ = 7 Hz; 8.4 Hz, $^4J_{H-H}$ = 1.4 Hz), 7.18 (m, 1H, H6, $^3J_{H-H}$ = 7 Hz; 7.9 Hz, $^4J_{H-H}$ = 1 Hz), 6.70 (d, 1H, H3, $^3J_{H-H}$ = 9.4 Hz), 4.36 (d,1H, H12), 4.31 (m, 1H, H14), 1.14 (d, 3H, H15, $^3J_{H-H}$ = 6.4 Hz). ^{13}C NMR (DMSO, ppm): δ = 178.6 (C2), 171.2 (C13), 159.2 (C11), 137.7 (C4), 134.6 (C9), 129.0 (C5), 128.1 (C7), 126.1 (C3), 125.2 (C10), 122.3 (C6), 118.3 (C8), 105.8 (C1), 68.9 (C12), 66.6 (C14), 20.5 (C15). $[\alpha]_D^{20}$ = -10.5° (0.2g/100 ml DMSO). UV-Vis in DMSO, λ [nm] (ε in l/(mol*cm)): 306 (13630), 404 (13010), 424 (13950). Anal. calcd. for $C_{15}H_{15}NO_4$: C 65.91, H 5.54, N 5.13; found: C 66.18, H 5.56, N 5.10.

2.5 X-ray structure analyses

Single crystals of the compounds suitable for X-ray structure analysis were grown from methanol solution at 276 K, mounted on a glass fiber and transferred to the nitrogen gas stream of the diffractometer (Stoe IPDS 2T; graphite-monochromated Mo-K_α radiation, λ = 0.71073 Å). The structures were solved by direct methods (SHELXS97) [37] and refined by full-matrix least-squares methods on F^2 for all unique reflections (SHELXL2014) [38]. The position of the hydrogen atom between the phenolic oxygen atom O1 and the nitrogen atom N1 was identified from residual electron density in a final stage of the refinement process in all three compounds (**1-3**). Refinement of this hydrogen atom position was performed without any restraints. The position of the carboxylic hydrogen atoms in **1-3** and the hydrogen atom of the threonine group in **3** was also localized from residual electron density. All other hydrogen atoms were positioned geometrically and refined with a riding model. The compounds **1-lt**, **1-ht**, and **3** crystallize in the chiral space group $P2_1$. The Flack-parameter for these structures is not reliable, since these are light atom structures. Crystallographic data are summarised in Table 1.

Table 1: Crystallographic Data of Compounds **1-lt**, **1-ht**, **2**, and **3**.

	1-lt	**1-ht**	**2**	**3**	**3** [39]
Empirical formula	$C_{16}H_{17}NO_3$	$C_{16}H_{17}NO_3$	$C_{20}H_{17}NO_3$	$C_{15}H_{15}NO_4$	
Formula weight	271.31	271.31	319.35	273.28	
T (K)	153(2)	253(2)	294(2)	153(2)	r.t.
λ (Å)	0.71073	0.71073	0.71073	0.71073	
Crystal system	monoclinic	monoclinic	monoclinic	monoclinic	
Space group	$P2_1$	$P2_1$	$P2_1/c$	$P2_1$	
a (Å)	16.194(1)	5.3493(5)	13.908(1)	5.0640(2)	5.109(2)
b (Å)	10.243(1)	10.4044(1)	10.761(1)	11.2479(4)	11.334(2)
c (Å)	16.703(1)	12.7115(1)	11.323(1)	11.0867(4)	11.155(3)
α (°)	90	90	90	90	
β (°)	93.609(4)	94.690(7)	108.041(4)	91.590(2)	91(3)
γ (°)	90	90	90	90	
Volume ($Å^3$), Z	2765.1(3), 8	705.11(7), 2	1611.27(4), 4	631.25(4), 2	645.8(3), 2
Calculated density ($g\ cm^{-3}$)	1.303	1.278	1.316	1.438	1.405
Absorption coefficient (mm^{-1})	0.090	0.088	0.089	0.105	0.103
F(000)	1152	288	672	288	
θ Range for data collection (°)	2.52-27.09	3.22-27.42	1.54-27.50	2.58-28.00	
Limiting indices	-20<h<20	-6<h<6	0<h<18	-6<h<6	
	-13<k<13	-13<k<13	-13<k<13	-14<k<14	
	-21<l<21	-16<l<16	-14<l<13	-14<l<14	
Data/restraints/ parameters	11815/4/777	3160/33/216	3705/1/234	3042/1/194	1373/-/-
Total/unique reflections	23665/11815	6676/3160	7203/3705	15115/3042	
R_{int}	0.0696	0.0315	0.0302	0.0206	
Completeness	99.5	99.8	100.0	99.9	
Refinement method	Full-matrix least squares on F^2				
Goodness-of-fit on F^2	1.09	1.089	0.990	1.05	
Final R index [l>2σ(l)]	R1 = 0.0506, wR2 = 0.0899	R1 = 0.0406, wR2 = 0.0887	R1 = 0.0398, wR2 = 0.0987	R1 = 0.0266, wR2 = 0.0713	R1 = 0.0438, wR2 = 0.1058
R index [all data]	R1 = 0.0921, wR2 = 0.1077	R1 = 0.0599, wR2 = 0.1010	R1 = 0.0568, wR2 = 0.1069	R1 = 0.0272, wR2 = 0.0719	
Largest difference peak/ hole ($e\ Å^{-3}$)	0.172/ -0.176	0.159/ -0.143	0.191/ -0.175	0.214/ -0.173	0.286/ -0.274

2.6 Quantum chemical calculations

The DFT calculations were carried out using GAUSSIAN 09 [40]. Geometries were fully optimized at the density functional theory level (DFT), using Becke's three-parameter hybrid exchange functional and the correlation functional of Lee, Yang and Parr (B3LYP) [41, 42]. Geometry optimizations and harmonic frequencies were calculated for all elements with the polarized 6-31G(d,p) basis set [43, 44, 45].

Relaxed potential energy surface scans have been performed with the Opt=ModRedundant utility in Gaussian 09 with B3LYP/6-31G(d,p). This option includes the specification of redundant internal coordinates. In these cases, a specific torsion angle has been changed in 5 degree steps. On every step the geometry of the molecule was completely optimized, restricting only the torsion angle to the specified value. This method allows access to a defined section of the potential energy surface.

Solvent model was applied with the polarizable continuum model (PCM) [46]. The same methodology as for the gas phase structures was applied here.

3. Results and discussion

The compounds **1**-**3** (Figure 1) were prepared similar to procedures previously described in the literature [29, 35].

3.1 X-ray structures

ORTEP-drawings of **1-ht**, **1-lt**, **2**, and **3** with atomic numbering schemes are shown in Figures 2, 3, 5, and 6. A summary of crystallographic data can be found in Table 1. During the X-ray diffraction experiment on *N*-(2-hydroxy-naphthylidene)-L-valine (**1**), a reversible phase transition was observed at 231 K. The temperature of the phase transition was determined on the diffractometer by repeated cell determinations at different temperatures. On cooling down the crystal below the phase transition temperature new reflections arose which lead to a quadruple cell volume. The phase transition is fully reversible, since the cell determination was repeated several times above and below the transition temperature. All investigations have been performed with the same crystal. The high- and low-temperature forms of **1** have been investigated in detail. The crystal structure of the high-temperature phase has been determined at 253 K (**1-ht**) and the structure of the low-temperature phase at 153 K (**1-lt**). The high-temperature form **1-ht** crystallizes in the monoclinic space group $P2_1$ with one crystallographic independent molecule in the asymmetric unit. The isopropyl group is

disordered (Figure 2). An intramolecular hydrogen bond is formed between N1-H1A···O1 The distance N1···O1 is 2.547 Å and the angle N1-H1A-O1 is 143°. A second contact might be discussed between N1-H1A···O2 with N1···O2 = 2.651 Å and N1-H1A-O2 = 82°. The long distance N1···O2 and the acute angle hints to a weak interaction. There is one intermolecular hydrogen bond present in the crystal lattice, i.e. O3-H···O1 with a distance O3···O1 of 2.509 Å and an O3-H···O1 angle of 175°. This interaction influences also the molecular conformation.

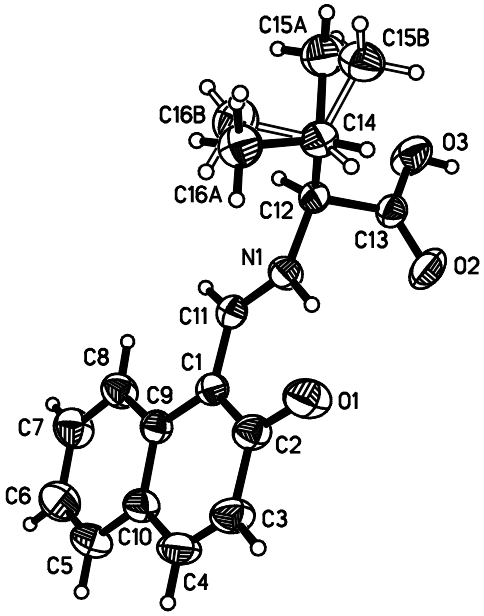

Figure 2: Molecular structure of high temperature form **1-ht** showing the atomic numbering scheme. The thermal ellipsoids of the non-hydrogen atoms are drawn at the 50% probability level.

The low-temperature form **1-lt** also crystallizes in the monoclinic space group $P2_1$. The unit cell contains four crystallographically independent molecules (Figure 3). These molecules can be described as four different conformational isomers. According to Buerger [47], **1** undergoes an order-disorder phase transition which is described as different atoms occupying the same crystallographic sites or the same atoms statistically occupying different crystallographic sites. The lengths of chemically equivalent bonds of the four molecules do not differ significantly from each other. The bond lengths are also similar to the bond lengths in **1-ht** (Table 2). Due to the flexibility of the *i*-propyl group the four molecules differ by torsion angles (Table 3) of the amino acid group. Newman projections of the *i*-propyl group in **1-lt** molecules are shown in Figure 4. Molecules **a** and **d** are represented by the left drawing and molecules **b** and **c** by the right drawing, respectively.

Similar as in the high temperature form bifurcated intramolecular hydrogen bonds are found in the low temperature form. The shorter interaction (major component) is always between the keto oxygen atoms bound to the naphthylidene ring and the imine hydrogen atom. Distances

vary from 2.537 Å for N2···O4 to 2.581 Å for N4···O10. The angles N-H···O are between 138 and 140°. Longer N···O distances between 2.561 and 2.753 Å and acute angles from 78 to 86° are observed for the interaction between the imine hydrogen and one oxygen atom of the carboxyl group (minor component). Therefore this part of the bifurcated hydrogen bonds should be classified as very weak contacts. There exist intermolecular hydrogen bonds between the carboxyl group of one Schiff base molecule and the oxygen atom at the naphthylidene group of an adjacent Schiff base conformer. This is essentially the same intermolecular interaction as in **1-ht**. The oxygen-oxygen distances vary between 2.519-2.551 Å and the oxygen-hydrogen-oxygen angles between 161 and 175°.

Table 2: Selected bond lengths [Å] and angles [°] of molecules **1-ht**, **1-lt**, **2**, and **3**.

	1-ht	**1-lt** [a)]				**2**	**3** (Özcan [39])
		a	**b**	**c**	**d**		
O1-C2	1.295(4)	1.292(5)	1.301(5)	1.309(5)	1.291(5)	1.300(2)	1.300(2) (1.30(3))
C1-C2	1.427(4)	1.439(5)	1.432(6)	1.429(6)	1.438(6)	1.420(2)	1.428(2) (1.43(1))
C1-C11	1.413(4)	1.421(6)	1.415(6)	1.416(5)	1.415(5)	1.410(2)	1.416(2) (1.402(5))
C11-N1	1.304(3)	1.311(5)	1.309(5)	1.314(5)	1.311(5)	1.303(2)	1.307(2) (1.31(3))
N1-C12	1.460(3)	1.461(5)	1.459(5)	1.450(5)	1.460(5)	1.457(2)	1.449(2)
C12-C13	1.538(4)	1.536(5)	1.534(6)	1.548(6)	1.528(5)	1.523(2)	1.540(2)
C12-C14	1.543(4)	1.547(6)	1.547(6)	1.552(5)	1.553(5)	1.539(2)	1.543(2)
C14-C15	1.580(1) 1.515(6)	1.524(6)	1.523(6)	1.532(6)	1.535(6)	1.511(2)	1.513(2)
C13-O2	1.205(3)	1.218(4)	1.213(5)	1.215(5)	1.220(5)	1.300(2)	1.300(2)
C13-O3	1.299(4)	1.307(5)	1.315(5)	1.311(5)	1.317(5)	1.203(2)	1.218(2)
C1-C2-O1	121.0(3)	121.2(3)	121.0(3)	121.2(4)	120.9(4)	121.0(1)	120.9(1)
C11-C1-C2	119.3(3)	119.1(4)	119.2(4)	119.5(4)	119.4(4)	119.7(1)	119.3(1)
C1-C11-N1	123.8(3)	123.8(4)	123.3(4)	123.3(4)	124.6(4)	124.9(1)	122.2(1)
C11-N1-C12	126.4(2)	125.8(4)	126.0(4)	126.4(4)	124.8(4)	124.0(1)	128.1(1)
N1-C12-C13	106.7(2)	108.3(3)	107.3(3)	107.5(3)	107.8(3)	112.1(1)	110.7(1)
N1-C12-C14	109.5(2)	109.3(3)	111.2(3)	112.0(3)	108.7(3)	111.5(1)	107.6(1)
C12-C13-O2	122.2(3)	122.4(4)	122.4(4)	121.6(4)	122.7(4)	114.5(1)	112.0(1)
C12-C13-O3	113.0(2)	112.8(3)	112.6(3)	113.1(3)	112.9(3)	120.7(1)	122.2(1)
C12-C14-C15	104.8(6) 115.4(3)	109.9(4)	109.8(3)	110.3(3)	110.1(3)	114.0(1)	113.6(1)

[a)] Equivalent bonds and angles have been used for the crystallographic independent molecules of **1-lt**.

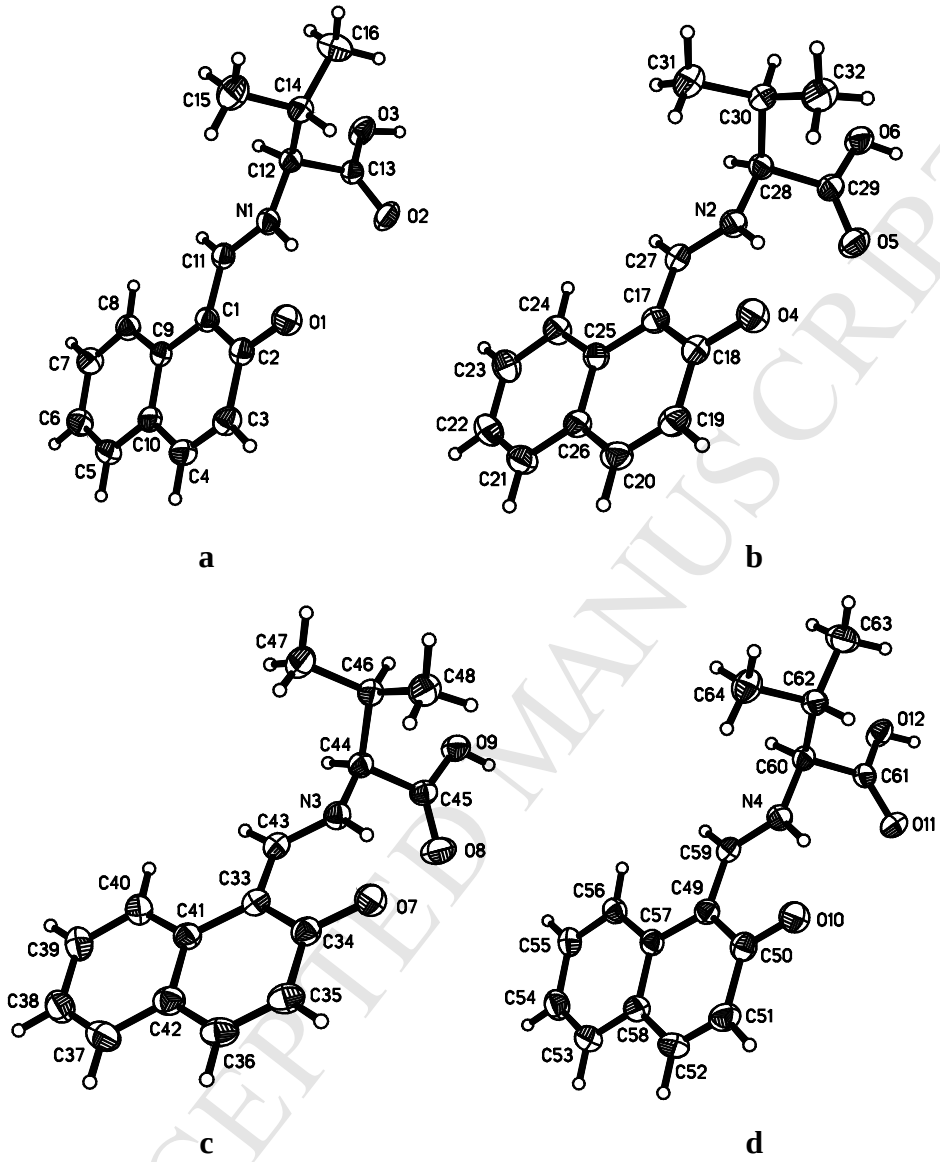

Figure 3: Molecular structures of the crystallographic independent molecules **a**-**d** of the low temperature form **1-lt** showing the atomic numbering scheme. The thermal ellipsoids of the non-hydrogen atoms are drawn at the 50% probability level.

Table 3: Torsion angles [°] of the four crystallographically independent molecules in **1-lt** and **1-ht**.

	1-lt [a)]				**1-ht**
	molecule **a**	molecule **b**	molecule **c**	molecule **d**	
C9-C1-C11-N1	-176.2(4)	-176.1(4)	-177.2(4)	-178.1(4)	-176.8(3)
C1-C11-N1-C12	172.5(4)	173.0(4)	175.2(4)	174.6(4)	172.0(3)
C11-N1-C12-C14	136.4(4)	117.1(4)	112.4(4)	129.3(4)	131.8(3)
N1-C12-C14-C15	-65.4(4)	-53.8(4)	-65.6(4)	-59.5(4)	-162.2(8).

					170.0(4)
N1-C12-C14-C16	170.5(3)	70.3(4)	58.5(4)	177.8(3)	-46.2(8). -63.7(5)
C11-N1-C12-C13	-102.0(4)	-118.9(4)	-121.6(4)	-107.5(4)	-106.0(3)
N1-C12-C13-O2	-24.7(5)	3.1(6)	16.0(6)	-15.0(5)	-17.2(4)
N1-C12-C13-O3	156.4(3)	-176.7(4)	-164.5(3)	164.7(3)	162.3(3)

[a)] Equivalent torsion angles have been used for the crystallographic independent molecules of **1-lt**.

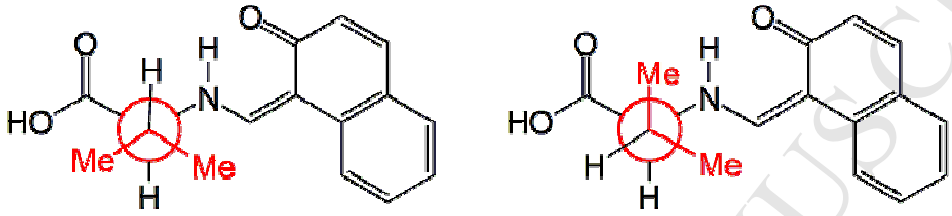

Figure 4: Newman-projections of the *i*-propyl group in **1-lt**. Molecules **a** and **d** refer to the left and **b** and **c** to the right projection, respectively.

N-(2-hydroxy-1-naphthylidene)-L-phenylalanine (**2**) crystallizes in the monoclinic space group $P2_1/c$ with one crystallographically independent molecule in the asymmetric unit (Figure 5). The lattice symmetry includes an inversion center, thus the compound is a racemic mixture. This is also shown by the optical rotation of 0° of the bulk material. Selected bond lengths and angles are given in Table 2. There is an intramolecular hydrogen bond between N1-H1A···O1 with a distance N1···O1 = 2.588 Å, and an angle N1-H1···O1 = 136°. A second contact might be discussed between N1-H1A···O2 with a distance N1···O2 = 2.627 Å and an angle N1-H1···O2 = 82°. These are supplemented by one intermolecular interaction between the carboxylic O2-H and the oxygen atom O1 at the naphthylidene group of a neighbouring molecule with a distance O1···O2 of 2.514 Å and an angle O2-H2···O1 of 173°. This interaction influences also the overall conformation of the molecule.

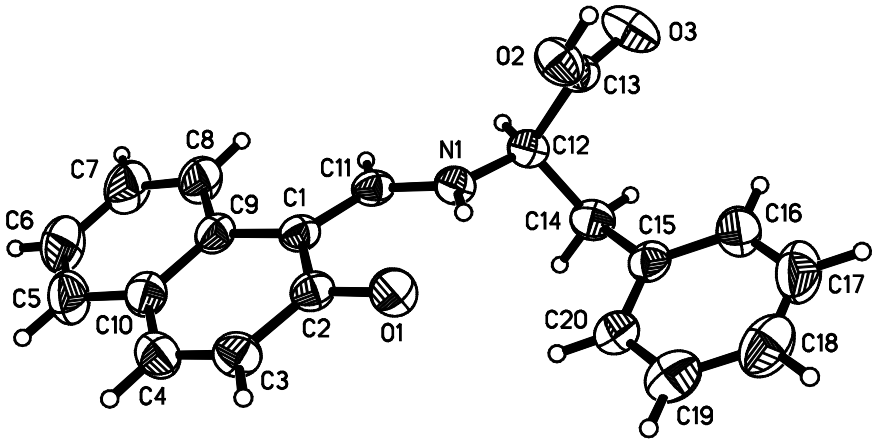

Figure 5: Molecular structure of **2** showing the atomic numbering scheme. The thermal ellipsoids of the non-hydrogen atoms are drawn at the 50% probability level.

N-(2-Hydroxy-naphthylidene)-L-threonine (**3**) crystallizes in the monoclinic space group $P2_1$ and with one crystallographically independent molecule in the asymmetric unit (Figure 6). A crystal structure analysis of *N*-(2-hydroxy-1-naphthylidene)-L-threonine was published already in 2003 by Özcan et al. [39]. Additionally we determined the value of optical rotation (see above) and offer a qualitatively improved crystallographic dataset of the compound (R_1 = 2.66% and R_2 = 2.72% vs. R_1 = 4.38% and R_2 = 10.58%). There is a bifurcated intramolecular hydrogen bond between N1-H1A···O1 (major component) and N1-H1A···O4 (minor component) with distances N1···O1 = 2.516 Å, N1···O4 = 2.812 Å and angles N1-H1···O1 = 139°, N1-H1···O4 = 102°. There are two intermolecular hydrogen bonds which influence solid state packing and molecule conformation. The O2-H···O1 hydrogen bond is approximately equivalent to those in **1** and **2** and has a O2···O1 distance of 2.472 Å and an angle O2-H···O1 of 174°. Due to the additional hydroxyl group in the amino acid moiety, another intermolecular hydrogen bond between the threonine hydroxyl group O4-H4 and O3 is formed, with O3 referring to the double bound oxygen of the carboxylic group. The O4···O3 distance is 2.941 Å and the angle O4-H···O3 is 165°.

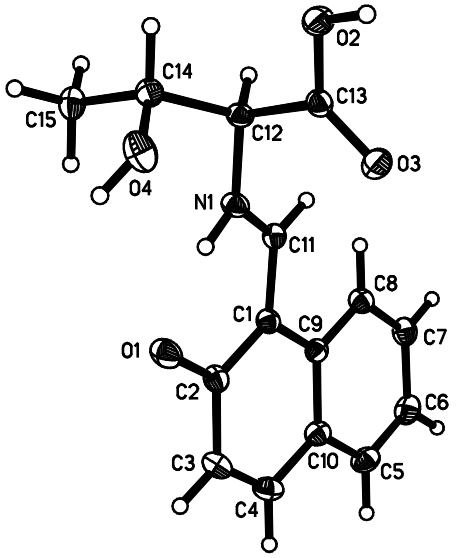

Figure 6: Molecular structure of **3** showing the atomic numbering scheme. The thermal ellipsoids of the non-hydrogen atoms are drawn at the 50% probability level.

Selected bond lengths and angles of compounds **1**, **2**, and **3** are given in Table 2. In general, the corresponding values do not differ significantly between these three compounds. The nature of the amino acid group does not have a substantial influence on the structural parameters. In **3**, the hydroxyl group in the amino acid unit causes more hydrogen bonds and therefore a tighter packing in the crystal structure.

3.2 Values of optical rotation

Values of optical rotation were determined with $[\alpha]_D^{20}$ = -109° (0.1 g / 100 ml DMSO) for **1**, $[\alpha]_D^{20}$ = 0° for **2** (1 g / 100 ml DMSO), and $[\alpha]_D^{20}$ = -10.5° (0.2 g/100 ml DMSO) for **3**. Therefore it can be assumed that **1** and **3** were prepared as chiral compounds under retention of the stereochemistry of the amino acid. In contrast to that compound **2** suffered from racemization. This process has already been observed for enantiomerically pure phenylalanine esters in MeCN/H_2O in presence of e.g. salicylaldehyde at pH 7, but not for the free phenylalanine in presence of 1-hydroxy-2-naphthaldehyde in slightly basic conditions [48]. Being not as activated for racemization processes as arylglycine amino acid derivatives, arylalanine equivalents are also able to stabilize the negative charge occurring after hydrogen abstraction from the asymmetric carbon (C12).

3.3 ^{1}H and ^{13}C NMR spectroscopy

In the ^{1}H NMR spectra recorded in DMSO-d_6 the hydrogen atom involved in the intramolecular hydrogen bond has the highest chemical shift (O1···H···N1; 14.49 ppm for **1**,

14.29 ppm for **2**, 13.82 ppm for **3**, for atom numbering see Figure 1) followed by the carboxylic hydrogen atom (13.37 for **1**, 13.44 for **2**, 13.11 for **3**). This high shift for O1···H···N1 hints towards a quite acidic hydrogen atom and therefore towards a hydrogen bridge. The signal for the imine hydrogen H11 appears around 9 ppm (9.15 ppm for **1**, 8.95 ppm for **2**, 9.02 ppm for **3**) and occurs at concentrations used for routine NMR characterization as a singlet in all cases presented herein. ^{1}H NMR shifts for hydrogen atoms H3-H8 are situated between 6.6 and 8.0 ppm. Signals at 4.34 ppm for **1**, 4.77 ppm for **2**, 4.36 ppm for **3** belong to the hydrogen atom H12 at the asymmetric carbon C12.

In **1** the multiplet at 2.33 ppm belongs to H14 and is caused by the coupling to the two diastereotopic methyl groups at about 0.96 ppm. The signal for H14 of **3** is at around 2.34 ppm as a multiplet due to coupling with H12 and the methyl group.

^{13}C NMR shifts characteristic for *N*-(2-hydroxy-1-naphthylidene)amino acids occur at about 172 ppm for the carboxylic carbon C13 (171.8 ppm for **1;** 171.7 ppm for **2**; 171.2 ppm for **3**), for C11 at 159.7 ppm for **1**; 159.5 ppm for **2**; 159.2 ppm for **3** and for C2 at 176.1 ppm for **1**; 174.9 ppm for **2**; 178.6 ppm for **3**. Nine signals between approximately 138 to 105 ppm belong to the aromatic carbon atoms C1 and C3-C10. The ^{13}C NMR chemical shift of C12 is 69.3 ppm, 65.2 ppm and 66.6 ppm for **1**, **2**, and **3** respectively. The two diastereotopic methyl groups of the amino acid in **1** show slightly different chemical shifts of 17.2 and 19.0 ppm. The chemical shift of the methyl group in **3** is found at 20.5 ppm.

These results are in accordance with literature data [49, 50].

*3.4 Intramolecular hydrogen bonding and tautomerism in naphthylidene amino acid Schiff bases **1-3***

Phenol-imine (**PI**) and keto-amine structures (**KA**, Figure 7) may occur in *N*-(2-Hydroxy-1-naphthylidene)amino acids and related salicylaldimine Schiff bases. This form of intramolecular tautomerism has been discussed in numerous papers (For reviews and general papers about this subject see [51, 52, 53, 54, 55] and literature cited therein). The electronic absorption spectra of several *N*-(2-Hydroxy-1-naphthylidene)amino acids derived from glycine, alanine, leucine, valine, and phenylalanine have been investigated in various solvents by Ebead et. al. [35]. They stated that these compounds should exist predominately or completely in the keto-amine form in solution. In contrast to that, Özcan et al. [39] found the phenol-imine form in the solid state structure of *N*-(2-Hydroxy-1-naphthylidene)-l-threonine (**3**). All hydrogen atoms were geometrical positioned in this previous structure determination and refined with a riding model. For us it seems not appropriate to decide about the nature of

a tautomer on the basis of a geometrical positioned hydrogen atom. Therefore we were motivated to have a closer look at the solid state structures of *N*-(2-Hydroxy-1-naphthylidene)amino acids.

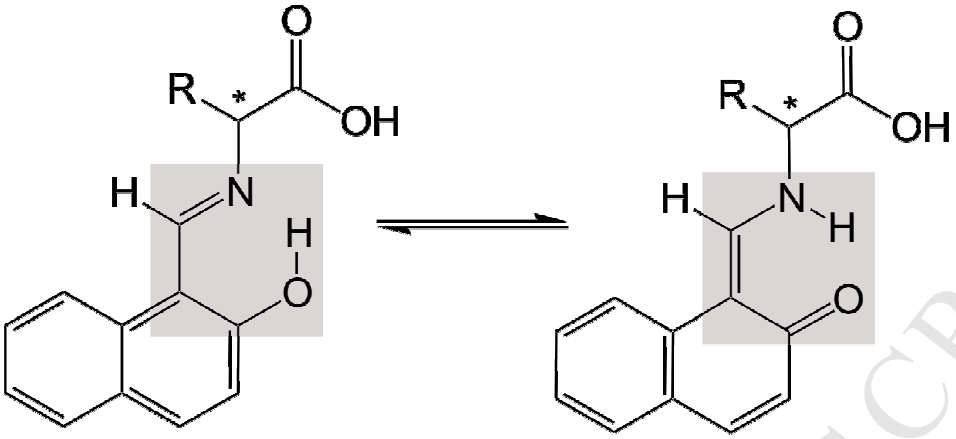

PI **KA**

Figure 7: Phenol-imine (**PI**) and keto-amine (**KA**) tautomeric form of N-(1-hydroxy-1-nyphthylidene)amino acids.

3.4.1 Discussion of the X-ray structural data

The X-ray structure analyses of **1-3** deliver experimental facts about the preferred tautomeric form in the solid state. The position of the hydrogen atom between the phenolic oxygen atom O1 and the nitrogen atom N1 was identified from residual electron density during the refinement process of all three X-ray structures. The further refinement without any restraints indicates that the hydrogen atom is localised close to the nitrogen atom, thereby forming the **KA** structure. However, one might argue that the position of hydrogen atoms cannot be determined reliable during the X-ray experiment [56]. Therefore the bond lengths between the surrounding non-hydrogen atoms O1-C2, C2-C1, C1-C11, and C11-N1 were included into the discussion in order to obtain a reliable decision which tautomer is present in the solid state structures. As can be seen in Table 2, these bond lengths do not vary significantly between the X-ray structures of **1-ht**, **1-lt**, **2**, and **3**. Therefore, we conclude that all three Schiff bases have the same tautomeric form in solid state.

Bond lengths statistics for both tautomeric forms were drawn from the Cambridge Structural Database [57] in order to decide which tautomer is present in the solid state structures of **1-3**. For this purpose the fragments shown in Figure 8 have been drawn and searched for in the

CSD. Please notice that these structural fragments include all *N*-(2-hydroxy-1-naphthylidene)- and *N*-(2-hydroxy-1-salicylaldimine)-derivatives. There were 1998 hits for the phenol-imine form (**PI**) and 104 hits for the keto-amine form (**KA**). The bond lengths shown in Figure 8 should vary considerably from **PI** to **KA** form due to the alternating bond character between formal single and double bonds. Indeed there are significant differences between the bond lengths in both forms (Table 4). The comparison with the mean values of the bond lengths of **1-3** shows undoubtedly the presence of the **KA** form. On the basis of this statistical analysis we can conclude that the tautomeric form assigned by Özcan et al. [39] for **3** was wrong.

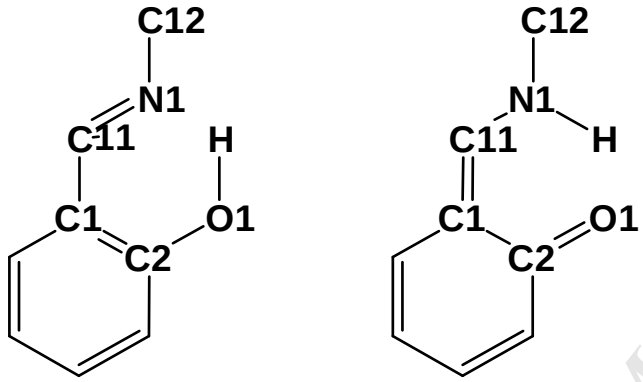

Figure 8: Schematic drawing of phenol-imine (**PI**) and keto-amine (**KA**) form in *N*-(2-hydroxy-1-naphthylidene)- and *N*-(2-hydroxy-1-salicylaldimine)-derivatives.

Table 4: Statistical Data from the CSD for the tautomers shown in Figure 8 and mean values for the X-ray structures **1-ht**, **2**, and **3** in Å.

Tautomer	**O1-C2**	**C2-C1**	**C1-C11**	**C11-N1**
phenol-imine *	1.343	1.406	1.450	1.286
keto-amine *	1.291	1.431	1.414	1.303
mean values **1-3**	1.298	1.425	1.414	1.305

*CSD search for distances, CSD version 5.36 (november 2014), search parameters: only organics.

3.4.2 Considerations regarding ^{1}H and ^{13}C NMR spectroscopy in solution

In order to determine the existing tautomeric structure of Schiff bases in solution ^{1}H and ^{13}C NMR spectroscopic experiments were already successfully performed on salicylaldehyde [53, 58, 59] and 2-hydroxy-1-naphthaldehyde derived Schiff bases [49, 50, 58]. In general, the most characteristic NMR signals are that of imine hydrogen atom H11 and carbon atom C2 with regard to chemical shift and signal form. In ^{1}H NMR spectra of the **PI** form the signal of

imine hydrogen atom H11 appears as a singlet, whereas in the **KA** form a doublet is formed due to the $^{3}J_{H\text{-}H}$ coupling to the hydrogen atom bound at N1. The signal of carbon atom C2 shifts downfield due to the change from a phenolic carbon, which is part of an aromatic system, to a carbonyl carbon atom in the **KA**. From these observations in the spectra about position and splitting of the signals it should be possible to draw a conclusion about the predominant tautomeric form in solution.

Detailed ^{1}H and ^{13}C NMR spectroscopic experiments were performed using **1** as an example. In DMSO solutions at concentrations used for routine characterization (about 10 mg/ml) H11 appears as a slightly broadened singlet, hydrogen N1-H-O1 as well as the carboxylic hydrogen as a broad singlet.

The increased linewidth of these signals indicates inter- and/or intramolecular exchange processes between the acidic hydrogen atoms of the compounds including the N1···H environment. To reduce the exchange rate low temperature NMR measurements as presented by Rozwadowski et al. [53] were intended in solvents having suitable melting points. For comparability with the results from 5-nitrosylaldehyde derived Schiff bases [53] we first chose chloroform as solvent. Unfortunately **1** has a very low solubility in chloroform making the record of ^{13}C NMR spectra impossible.

In the ^{1}H NMR spectrum of **1** in deuterated acetone the signal of the imine hydrogen H11 appears even in highly concentrated solutions as a sharp singlet at 9.3 ppm, those of the acidic hydrogens appear as very broad singlets. The ^{13}C NMR signal of C2 has a shift of 172.1 ppm, thus beeing significantly upfield compared to the chemical shift of C2 obtained in the solid state CP MAS spectrum for the **KA** form with 178.6 ppm. Both indicate that the equilibrium (see tautomeric forms in Figure 7) in acetone solution is on the side of the **PI** structure. For that reason and as it was questionable if the achievable temperatures would be sufficient to reduce the exchange rate to the slow exchange mode on the NMR time scale variable-temperature NMR experiments did not seem promising.

Compound **1** shows a good solubility in DMSO. As the observed proton exchange reactions can be both inter- as well as intramolecular, it was intended to reduce the less interesting intermolecular exchange rates by diluting the solution. Therefore we performed NMR measurements in the concentration range 0.4 – 40 mg/ml in DMSO-d_6 at 400.13 MHz.

At concentrations of ≥ 20 mg / ml no splitting of the imine hydrogen H11 signal but an increased linewidth compared to the aromatic protons is observed. Splitting starts at 10 mg / ml.

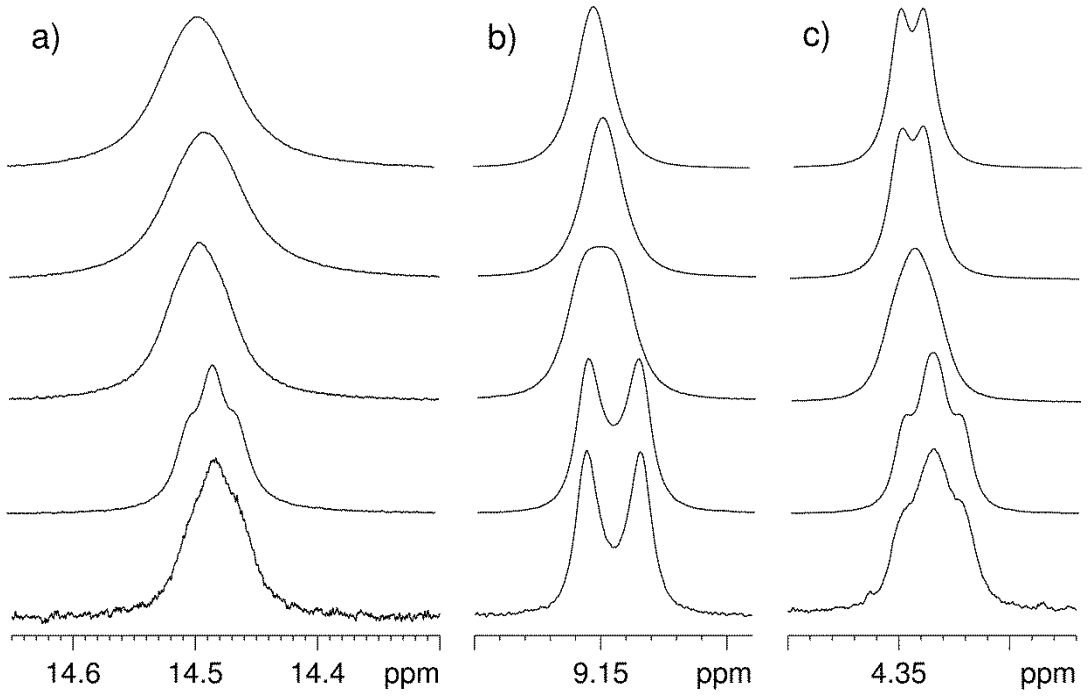

Figure 9: Parts of the ^{1}H NMR spectra of **1** in DMSO at different concentrations (from top to bottom: 40 mg, 20 mg, 10 mg, 2 mg, 0.4 mg / ml DMSO): a) phenol hydrogen O1-H; b) imine hydrogen H11; c) hydrogen atom H12 at asymmetric carbon atom C12. Signals are scaled to comparable intensity.

At concentrations of 2 mg/ml and 0.4 mg/ml DMSO splitting of hydrogen signals H11 (s → d), phenol hydrogen O1-H (s → t) and hydrogen atom H12 (d → t) is observed (Figure 9), indicating that the phenolic proton is interacting with N1 giving rise to a coupling to H11 and H12. For the lowest concentration a coupling constant of 8.4 Hz can be determined for the H11 doublet. Additionally, the carboxyl hydrogen signal gets narrower with decreasing concentrations. As expected in low concentrated solutions the intermolecular exchange between the hydroxyl protons is reduced resulting in a longer dwell time of the hydrogen atom in the intramolecular hydrogen bridge O1···H···N1, thus H-H coupling to H11 and H12 can now be made visible by H,H COSY NMR (Figure 10) and the coupling constant can be determined.

The ^{13}C NMR signal of the phenol carbon atom C2 did not experience significant changes by changing concentrations. In conclusion it can be stated that the tautomeric equilibrium is not noticeable influenced by the concentration of the solution.

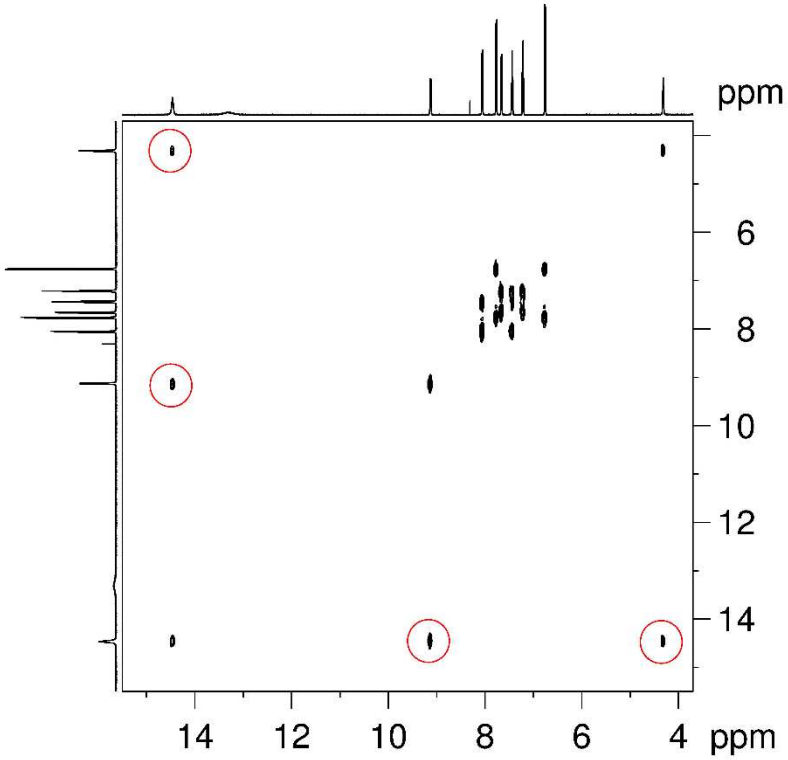

Figure 10: Section of the H,H COSY NMR spectrum of **1** (2 mg/ml in DMSO) showing coupling of phenol hydrogen O1-H and the hydrogen atoms H11 (imine) and H12 (N-C*H).

Interestingly the splitting for H11, H12 and O1-H can also be induced by the use of wet DMSO. Here the water quickly exchanges with the carboxyl groups, reducing the exchange between the carboxyl group and the hydrogen in O1···H···N1. Thus the intramolecular hydrogen bridge O1···H···N1 is stabilized.

A share of 62 to 64 % KA form can be estimated from the values of $^{3}J_{H\text{-}H}$ coupling at H11 (8.4 Hz compared to 13.1 Hz for molecules in pure KA form [53, 58]) and the ^{13}C NMR shift of carbon atom C2 with 176.2 ppm (compared to 178.6 ppm for the KA form in solid state and 172.1 ppm for the PI form in aceton), respectively, at room temperature in DMSO. These values fit – within the experimental error- very nicely to the results obtained by UV/VIS spectroscopy.

By heating the solution of **1** with a concentration of 40 mg / ml DMSO an increasing proton exchange between the carboxylic group and the intramolecular hydrogen bond is observed by broadening of their hydrogen signals COOH and O1···H···N1. The signals of imine hydrogen H11 and of H12 become sharper and are shifted towards higher field (Figure 11).

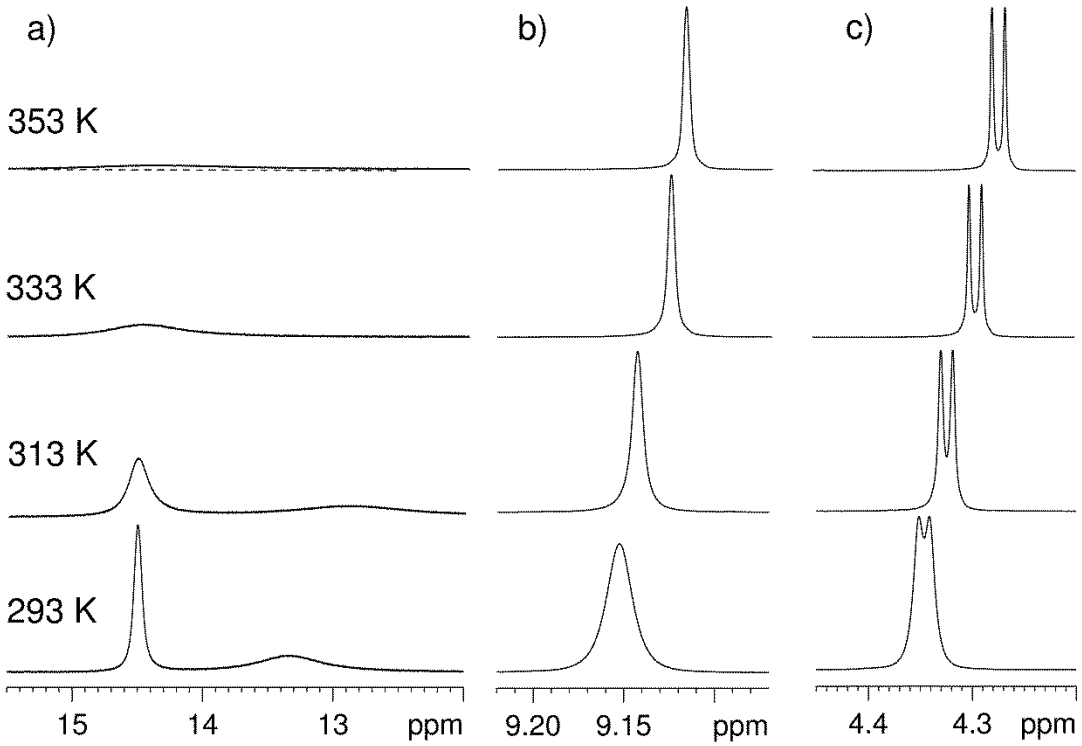

Figure 11: Parts of the ^{1}H NMR spectra of **1** in DMSO (40 mg/ml) at different temperatures; a) phenol hydrogen O1···H and H of the carboxylic acid; b) imine hydrogen H11; c) H12 at asymmetric carbon atom C12.

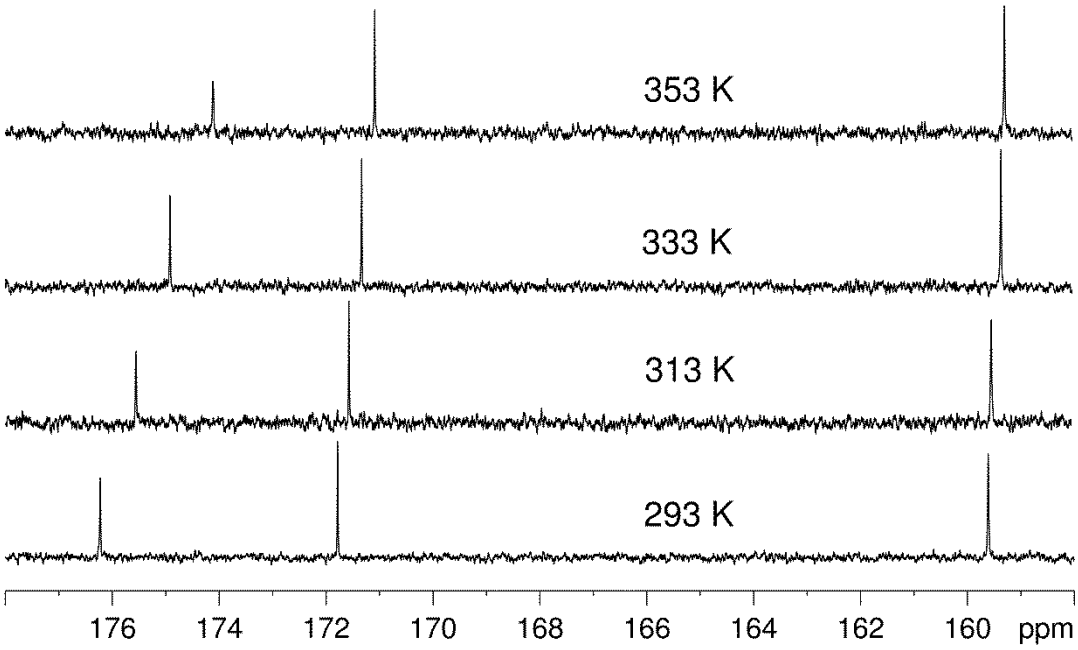

Figure 12: Part of the ^{13}C NMR spectra of **1** in DMSO solution (40 mg/ml) at different temperatures; from the left: carbon atom C2; carboxyl carbon C13; imine carbon C11.

Now also in ^{13}C NMR spectra a high field shift of all signals can be observed which is especially strong for phenol carbon atom C2 (Figure 12, 20 °C: δ (^{13}C) = 176.2 ppm, 80 °C: δ (^{13}C) = 174.1 ppm). This indicates that the **PI** / **KA** equilibrium is moving towards the phenol-imine side (Figure 7) with increasing temperature.

3.4.3 UV-Vis spectra

Tautomeric equilibria in Schiff bases have been already investigated with UV-Vis spectroscopy [60, 61]. It was shown in the literature that bands at ca. 300 nm indicate the presence of the phenol-imine form and bands above 400 nm the presence of the keto-amine form. UV-Vis spectra of **1**-**3** have been measured in DMSO. Therein both bands are observed in the expected regions and indicate that the compounds **1** and **2** consist of around 60 % keto-amine form (**KA**) in DMSO solution at room temperature. In compound **3** the keto-amine form prevails with 66%.

3.4.4 Quantum chemical calculations

Extensive quantum chemical analyses of tautomeric equilibria in ortho-hydroxyaryl Schiff bases have already been published [54, 62, 63,]. Quantum chemical calculations about the tautomerism in naphthylidene amino acid Schiff bases have recently been published by Ebead et al. [35]. Therein the authors made geometry optimizations at the PM6 and the B3LYP/6-31G** level of theory. However the geometries used by the authors seemed rather arbitrary and there were no information available about the potential energy surface and a possible transition state between phenol-imine and keto-amine form. Therefore we performed quantum chemical calculations with molecule **1** in order to gain further insight into the tautomerism in naphthylidene amino acid Schiff bases. The same DFT method / basis set combination as in [35] was used. Calculated molecules are denoted as $\mathbf{PI_{a-b}}$ for the phenol-imine and as $\mathbf{KA_{a-c}}$ for the keto-amine form. Geometries have been optimized in the gas phase and in DMSO solution.

3.4.4.1 Gas phase structures

The molecules **a** and **b** from the X-ray structure **1-lt** have been taken as starting point for optimization of the keto-amine form. These were optimized to two separate minima $\mathbf{KA_a}$ and

KA_b with zero imaginary frequencies. Both structures have nearly identical energies (Table 5). The keto-amin form published by Ebead [35] was also reoptimized and is denoted here as **KA_c**. This structure is 42.3 kJ/mol higher in energy than **KA_a** and **KA_b**. **KA_c** is indeed a local minimum on the potential energy surface, but it is not the global minimum. Furthermore the phenol-imine form was constructed by shifting the hydrogen atom in **KA_a** from the nitrogen atom to the oxygen atom. Geometry optimization and frequency calculation of this molecule gave **PI_a** as the global minimum. The phenol-imine form published by Ebead [35] was also reoptimized and is denoted here as **PI_b**. This structure is 66.0 kJ/mol higher in energy than **PI_a** and is also a local minimum on the potential energy surface. A schematic energy profile diagram for the calculated stationary points in the gas phase is shown in Figure 13.

Table 5: Relative energies of optimized molecule geometries at the B3LYP/6-31G(d,p) level.

	Gas phase structures	ΔG (kJ/mol)	in DMSO	ΔG (kJ/mol)
Keto-Amin Form	**KA_a**	4.2	**KA_a(DMSO)**	1.6
	KA_b	4.2	**KA_b(DMSO)**	0.0
	KA_c	46.5	**KA_c(DMSO)**	39.6
Transition state	**TS**	5.3	**TS(DMSO)**	7.5
Phenol-Imin Form	**PI_a**	0.0	**PI_a(DMSO)**	6.0
	PI_b	66.0	**PI_b(DMSO)**	62.2

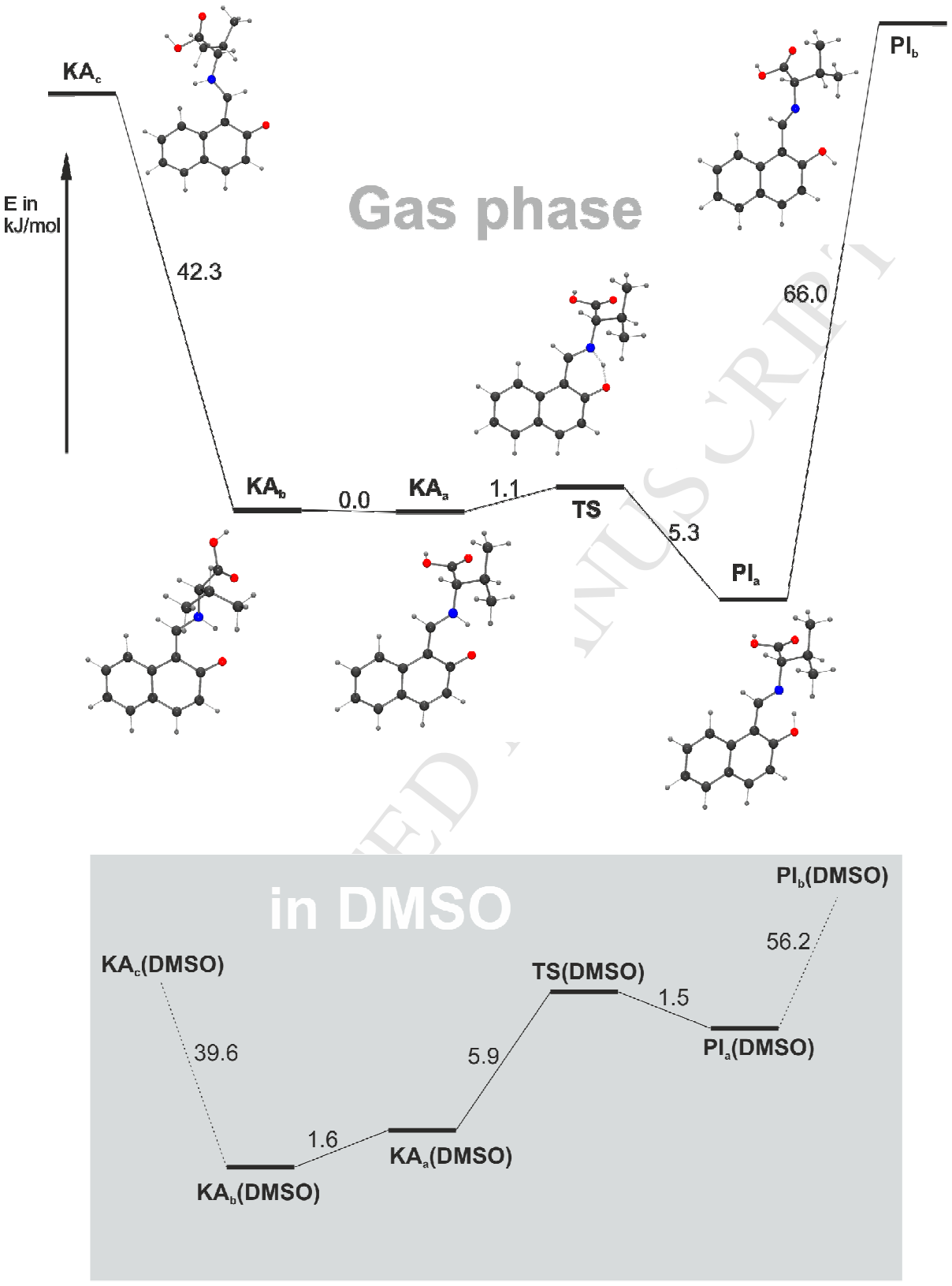

Figure 13: Schematic energy profile diagram for calculated stationary points in the gas phase (top) and in DMSO (bottom).

Relaxed potential energy surface scans for the gas phase structures of the keto-amine and the phenol-imine forms have been calculated by changing the torsion angle C2-C1-C11-N1 from 0 to 360°. Both PES are shown in Figure 14. As can be seen from the graph the lowest energy for both forms is reached at a torsion angle of zero degree. The structure **KA_c** has a torsion angle C2-C1-C11-N1 of 171.93 and represents therefore a local minimum on the PES in Figure 14. The torsion angle of **PI_b** is 33.26°. The slope of the torsion angle starting from zero degree is very low, therefore the frequency calculation pretends here a local minimum. The calculation of the PES proves that the minima published by Ebead [35] are local minima which do not represent the geometries with the lowest energy on the PES. From comparison of both graphs it becomes evident, that the global minimum for the gas phase structure is the phenol-amine form **PI_a** which is 4.2 kJ/mol lower in energy than the lowest energy form of the keto-imine form (**KA_a**/**KA_b**). This is in contrast to the X-ray structural data were the keto-imine form was obtained by crystallization from solution.

Additionally the transition state **TS** for the tautomeric process was calculated. It has a very low energy barrier with only 5.3 kJ/mol for the transformation from **PI_a** to **KA_a** (see Figure 13).

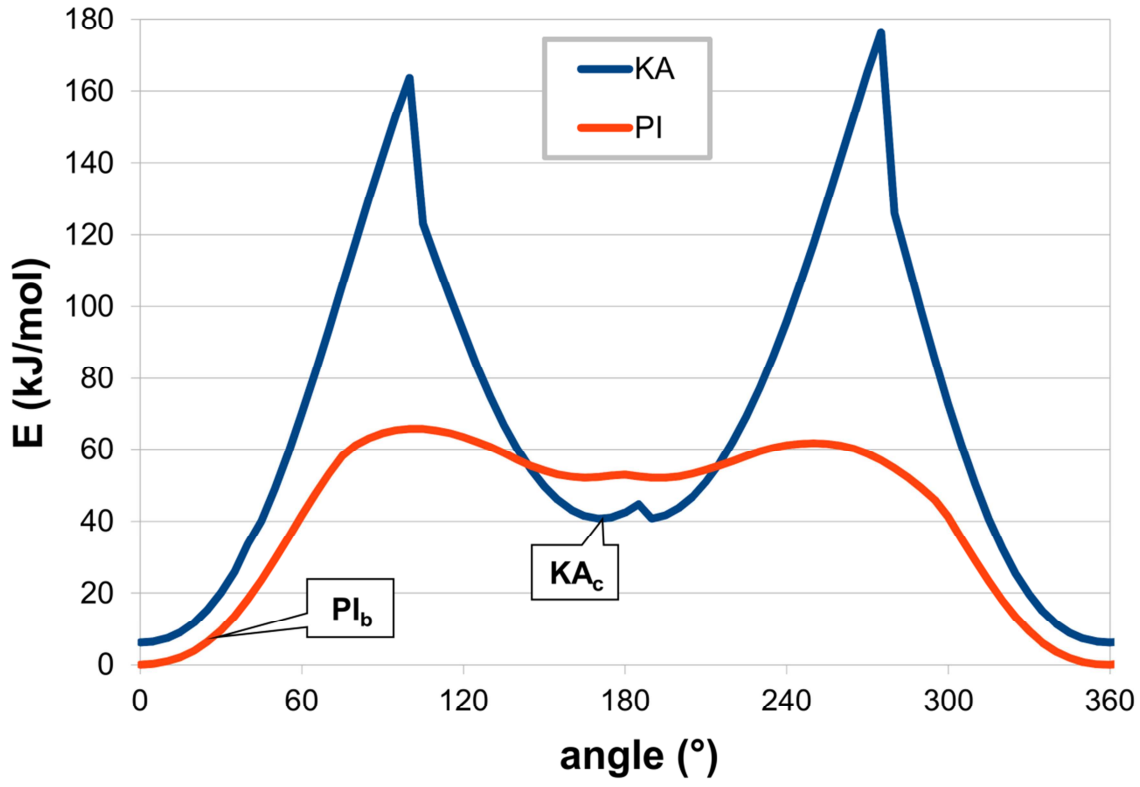

Figure 14: Potential energy surface scans for the keto-amin (**KA**) and the phenol-imine forms (**PI**) in the gas phase.

3.4.4.2 Structures in DMSO

The energy values are changing in DMSO solution. Herein the keto-amine form **KA_b(DMSO)** becomes the global minimum in this system (see Table 2 and Figure 13). The closely related geometry **KA_a(DMSO)** is 1.6 kJ/mol higher in energy. The phenol-imine form **PI_a(DMSO)** is 6.0 kJ/mol higher in energy. This energy difference implies that there should be a ratio of about 11:1 between keto-amine and phenol-imine form present in DMSO solution. Both forms published by Ebead [35] are again local minima with substantial higher energies. The transition state **TS(DMSO)** represents also in DMSO a low barrier for the transition from one form to the other. The independently calculated PES in DMSO solution prove these results (Figure 15). The lowest energy forms are observed at a torsion angle of zero degree. The keto-amin form is more stable in solution. This is experimentally proven by the fact that the chemical shift of C2 (δ= 176.1 ppm) in DMSO solution is very close to the value for the KA form observed in the solid state (δ= 178.6 ppm).

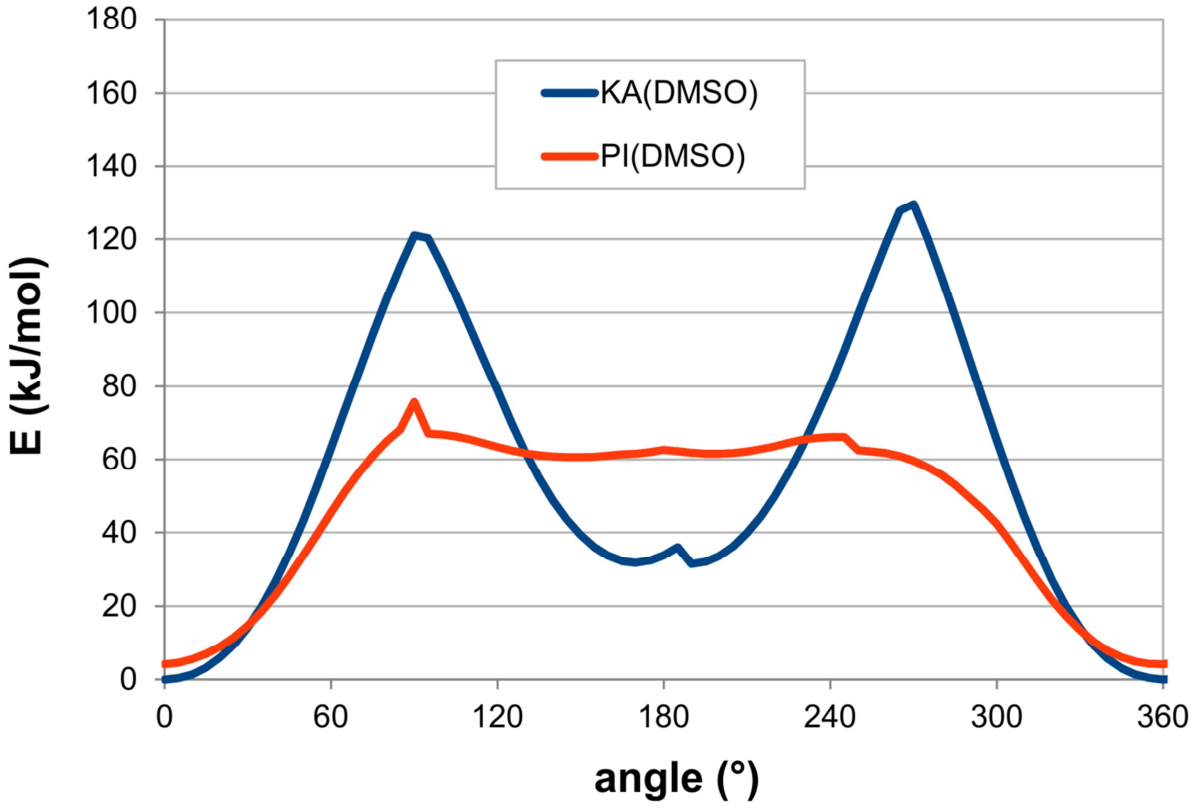

Figure 15: Potential energy surface scans for the keto-amin (**KA**) and the phenol-imine forms (**PI**) in DMSO solution.

Comparison of the PES scans in the gas phase (Figure 14) and in DMSO (Figure 15) shows that the phenol-imine form has in both media a barrier of ca. 60 kJ/mol for rotation around the torsion angle, whereas energy barrier for the rotation of the keto-amine form is lowered in solution to ca. 120-130 kJ/mol. Further local minima may arise from different orientations of the isopropyl and the carboxyl group at this molecule. But these have probably only minimal influence on the total energy of the molecule. The PES calculations presented here represent a good model to describe energy changes of compound **1**.

4. Conclusion

During our studies on Schiff base compounds derived from amino acids and 2-hydroxyaromatic aldehydes, we were able to prepare three *N*-(2-hydroxy-1-naphthylidene)amino acid derivatives. The crystal structures of *N*-(2-hydroxy-1-naphthylidene)-L-valine (**1**), *N*-(2-hydroxy-1-naphthylidene)-L-phenylalanine (**2**), and *N*-(2-hydroxy-1-naphthylidene)-L-threonine (**3**) uniformly exist in the keto-amine form in the solid state. The solid state structures are further stabilized by intra- and intermolecular hydrogen bonds. Equilibria between keto-amine and phenol-imine form are present in DMSO solutions of **1-3**. This was shown with ^{1}H NMR und UV-Vis spectra. According to NMR and UV-Vis data the keto-amine form prevails with about 60 to 66% in DMSO solution. The condition of tautomeric equilibrium depends mainly on the solvent and temperature but not on the concentration of the solution. With increasing temperature the equilibrium is shifted towards the **PI** form. The ^{1}H NMR spectra are affected by interfering intra- and intermolecular exchange processes, the rate of the latter can be reduced to the slow exchange mode with respect to the NMR frequency range by diluting the solution.

Quantum chemical calculations show that there are small energy differences between the keto-amine and the phenol-imine form in the gas phase and in DMSO solution. Calculation of the transition state shows, that there is only a small energy barrier below 10 kJ/mol for the transformation of one form to the other.

Coming back to the question from the headline of this paper we can state the following: The keto-amine form is more stable in room temperature DMSO solution and its existence was proven by ^{1}H NMR and UV-Vis. Therefore crystallization of the keto-amine form from solution is feasible.

5. Acknowledgements

The authors thank the Freistaat Sachsen for financial support and the computing centre of the TU Bergakademie Freiberg for computing time at the High Performance Compute Cluster. S.F. thanks the Freistaat Sachsen for a PhD fellowship (Sächsisches Landesstipendium).

Appendix A. Supplementary material

CCDC 1439783-1439786 contains the supplementary crystallographic data for this paper. These data can be obtained free of charge via ttp://www.ccdc.cam.ac.uk/conts/retrieving.html

6. References

1 M. Nath, S. Goyal, Phosphorus, Sulfur Silicon Relat. Elem. 177 (2002) 447-463.

2 T. M. Aminabhavi, N. S. Biradar, S. B. Patil, V. L. Roddabasanagoudar, Inorg. Chim. Acta 107 (1985) 231-234.

3 L. Tian, Z. Shang, X. Zheng, Y. Sun, Y. Yu, B. Qian, X. Liu, Appl. Organomet. Chem. 20 (2006) 74-80.

4 M. Jain, S. Gaur, V. P. Singh, R. V. Singh, Appl. Organomet. Chem. 18 (2004) 73-82.

5 M. Jain, S. Gaur, S. C. Diwedi, S. C. Joshi, R. V. Singh, A. Bansal, Phosphorus, Sulfur Silicon Relat. Elem. 179 (2004) 1517-1537.

6 M. Nath, R. Yadav, J. Therm. Anal. Calorim. 55 (1999) 135-142.

7 F. Mucha, U. Böhme, G. Roewer, Chem. Commun. 1998, 1289-1290.

8 F. Mucha, J. Haberecht, U. Böhme, G. Roewer, Monatsh. Chem. 130 (1999) 117-132.

9 J. Wagler, U. Böhme, G. Roewer, Angew. Chem. Int. Ed. 41 (2002) 1732-1734; corresponds to J. Wagler, U. Böhme, G. Roewer, Angew. Chem. 114 (2002) 1825-1827.

10 J. Wagler, U. Böhme, E. Brendler, B. Thomas, S. Goutal, H. Mayr, B. Kempf, G. Ya. Remennikov, G. Roewer, Inorg. Chim. Acta 358 (2005) 4270-4286.

11 U. Böhme, B. Günther, Inorg. Chem. Comm. 10 (2007) 482-484.

12 U. Böhme, S. Jähnigen, Acta Cryst. C64 (2008) o364–o366.

13 U. Böhme, J. Haushälter, Inorg. Chem. Comm. 12 (2009) 35-37.

14 U. Böhme, S. Fels, Acta Cryst. C66 (2010) o202-o205.

15 A. Schwarzer, L. E. H. Paul, U. Böhme, Acta Cryst., Sect C69 (2013) 1336-1339.

16 U. Böhme, S. Fels, Inorg. Chim. Acta 406 (2013) 251-255.

17 U. Böhme, S. Wiesner, B. Günther, Inorg. Chem. Comm. 9 (2006) 806-809.

18 G. Warncke, U. Böhme, B. Günther, M. Kronstein, Polyhedron 47 (2012) 46-52.

19 U. Böhme, S. Fels, Acta Cryst. C69 (2013) 44-46.

20 G. Y. Aly, M. K. M. Rabia, M. A. F. Al-Mohanna, Synth. React. Inorg. Met.-Org. Chem. 34 (2004) 45-66.

21 Y. Fujii, Y. Kuwana, S. Takahashi, K. Shimizu, K. Hiroi, Bull. Chem. Soc. Jpn. 55 (1982) 2598-2610.

22 I. Sakiyan, N. Gündüz, T. Gündüz, Synth. React. Inorg. Met.-Org. Chem. 31 (2001) 1175-1187.

23 I. Sakiyan, H- Yilmaz, Synth. React. Inorg. Met.-Org. Chem. 33 (2003) 971-983.

24 A. Dogan, I. Sakiyan, E. Kilic, Journal of Solution Chem. 33 (2004) 1539-1547.

25 I. Sakiyan, E. Logoglu, S. Arslan, N. Sari, N. Sakiyan, BioMetals 17 (2004) 115-120.

26 I. Sakiyan, R. Özdemir, H. Ögütcü, Synth. React. Inorg., Met.-Org., Nano-Met. Chem. 44 (2014) 417-423.

27 A. M. Shaker, L. A. E. Nassr, Int. J. Chem. Kinet. 35 (2003) 592-601.

28 A. M. Shaker, A. M. Aida, L. A. E. Lobna, Synth. React. Inorg. Met.-Org. Chem.33 (2003) 103-117.

29 L. H. Abdel-Rahman, R. M. El-Khatib, L. A. E. Nassr, A. M. Abu-Dief, F. E.-D. Lashin, Spectrochim. Acta, Part A 111 (2013) 266-276.

30 P. K. Sharma R. N. Handa, S. N. Dubey, Synth. React. Inorg. Met.-Org. Chem.26 (1996) 1219-1230.

31 M. R. Mahmoud, S. A. El-Gyar, A. A. Moustafa, A. Shaker, Polyhedron, 6 (1987) 1017-1020.

32 S. Y. New, X. Wu, S.-Q. Bai, L. L. Kon, T. S. A. H., F. Xue, Cryst. Eng. Comm. 13 (2011) 4288-4235.

33 M. Abdel-Moustafa, Bull. Pol. Acad. Sci., Chem. 43 (1995) 119-123.

34 R. Aman, G. Matela, E-Journal of Chem. 2013, 2013, 4pp.

35 Y. H. Ebead, H. M. A. Salman, M. A. Abdallah, Bull. Kor. Chem. Soc. 31 (2010) 850-858.

36 Z. Rozwadowski, K. Ambroziak, M. Szypa, E. Jagodzinska, S. Spychaj, W. Schilf, B. Kamienski J. Mol. Struct. 734 (2005) 137-142.

37 G. M. Sheldrick, Acta Crystallogr. A64 (2008) 112–122.

38 G. M. Sheldrick, Acta Crystallogr. C71 (2015) 3–8.

39 Y. Özcan, S. İde, İ. Şakıyan, E. Logoglu, J. Mol. Struct. 658 (2003) 207-213.

40 Gaussian 09, Revision B.01, M. J. Frisch, G. W. Trucks, H. B. Schlegel, G. E. Scuseria, M. A. Robb, J. R. Cheeseman, G. Scalmani, V. Barone, B. Mennucci, G. A. Petersson, H. Nakatsuji, M. Caricato, X. Li, H. P. Hratchian, A. F. Izmaylov, J. Bloino, G. Zheng, J. L. Sonnenberg, M. Hada, M. Ehara, K. Toyota, R. Fukuda, J. Hasegawa, M. Ishida, T. Nakajima, Y. Honda, O. Kitao, H. Nakai, T. Vreven, J. A. Montgomery, Jr., J. E. Peralta, F. Ogliaro, M. Bearpark, J. J. Heyd, E. Brothers, K. N. Kudin, V. N. Staroverov, T. Keith, R. Kobayashi, J. Normand, K. Raghavachari, A. Rendell, J. C. Burant, S. S. Iyengar, J. Tomasi, M. Cossi, N. Rega, J. M. Millam, M.

Klene, J. E. Knox, J. B. Cross, V. Bakken, C. Adamo, J. Jaramillo, R. Gomperts, R. E. Stratmann, O. Yazyev, A. J. Austin, R. Cammi, C. Pomelli, J. W. Ochterski, R. L. Martin, K. Morokuma, V. G. Zakrzewski, G. A. Voth, P. Salvador, J. J. Dannenberg, S. Dapprich, A. D. Daniels, O. Farkas, J. B. Foresman, J. V. Ortiz, J. Cioslowski, and D. J. Fox, Gaussian, Inc., Wallingford CT, 2010.

41 A. D. Becke, J. Chem. Phys. 98 (1993) 5648-5652.

42 P. J. Stephens, F. J. Devlin C. F. Chabalowski, M. J. Frisch J. Phys. Chem. 98 (1994) 11623-11627.

43 W. J. Hehre, L. Radom, P. R. Schleyer, J. A. Pople, Ab Initio Molecular Orbital Theory, J. Wiley & Sons, Chichester, 1986.

44 P. C. Hariharan, J. A. Pople, Theoret. Chimica Acta 28 (1973) 213-222.

45 M. M. Francl, W. J. Pietro, W. J. Hehre, J. S. Binkley, M. S. Gordon, D. J. DeFrees, J. A. Pople, J. Chem. Phys. 77 (1982) 3654-3665.

46 J. Tomasi, B. Mennucci, R. Cammi, Chem. Rev. 105 (2005) 2999-3094.

47 U. Müller, Anorganische Strukturchemie, 6. aktualisierte Auflage, Wiesbaden, Vieweg+Teubner, 2008, p. 55.

48 D. A. Schichl, S. Enthaler, W. Holla, T. Riermeier, U. Kragl, M. Beller, Eur. J. Org. Chem. (2008) 3506-3512.

49 S. R. Salman, J. C. Lindon, R. D. Farrant, T. A. Carpenter, Magn. Reson. Chem. 31 (1993) 991-994.

50 J. Matijević-Sosa, M. Vinković, D. Vikić-Topić, Croat. Chem. Acta 79 (2006) 489-495.

51 J. Costamagna, J. Vargas, R. Latorre, A. Alvarado, G. Mena, Coord. Chem. Rev. 119 (1992) 67-88.

52 R. M. Claramunt, C. Lopez, M. D. Santa Maria, D. Sanz, J. Elguero, Prog. Nucl. Magn. Reson. Spectrosc. 49 (2006) 169-206.

53 Z. Rozwadowski, T. Dziembowska, Magn. Reson. Chem. 37 (1999) 274-278.

54 A. Filarowski, J. Phys. Org. Chem. 18 (2009) 686-698.

55 S. Bilge, Z. Kilic, Z. Hayvali, T. Hökelek, S. Safran, J. Chem. Sci. (Bangalore, India) 121 (2009) 989-1001.

56 A. Ø. Madsen, Struct. Bond. 146 (2012) 21-52.

57 F. H. Allen, Acta Cryst. B58 (2002) 380-388.

58 Z. Rozwadowski, Magn. Reson. Chem. 44 (2006) 881-886.

59 P. Ossowics, E. Janus, G. Schroeder, Z. Rozwadowski, Molecules 18 (2013) 4986-5004

60 R. Herscovitch, J. J. Charette, E. de Hoffmann, J. Am. Chem. Soc. 95 (1973) 5135-5140.

61 H. Nazir, M. Yildiz, H. Yilmaz, M. N. Tahir, D. Ülkü, J. Mol. Struc. 524 (2000) 241-250.

62 M. Kluba, P. Lipkowski, A. Filarowski, Chem. Phys. Lett. 463 (2008) 426-430.

63 A. Filarowski, I. Majerz, J. Phys. Chem. A 112 (2008) 3119-3126.

Ms. Ref. No.: L12-49-15

Title: Tautomerism in N-(2-hydroxy-1-naphthylidene)amino acids and the search for an answer to the difficult question about where the proton belongs

Highlights

- Tridentate O,N,O'- Schiff bases with amino acid moieties were synthesized and characterized.
- Order-disorder phase transition occurs for *N*-(2-hydroxy-1-naphthylidene)-L-valine.
- All three Schiff bases exist uniformly in keto-amine tautomeric structure in solid state.
- NMR and UV-Vis spectroscopy show that the keto-amine form is slightly more stable in solution.